

# A proposal of anomaly detection method based on natural data augmentation in the Eigenspace

Naoki Murakami  
Chukyo University  
101-2 Yagoto-honmachi  
466-8666, Nagoya, Japan  
[murakami@asmi.sist.chukyo-u.ac.jp](mailto:murakami@asmi.sist.chukyo-u.ac.jp)

Naoto Hiramatsu  
Chukyo University  
101-2 Yagoto-honmachi  
466-8666, Nagoya, Japan  
[hiramatsu@asmi.sist.chukyo-u.ac.jp](mailto:hiramatsu@asmi.sist.chukyo-u.ac.jp)

Kobayashi Hiroki  
Chukyo University  
101-2 Yagoto-honmachi  
466-8666, Nagoya, Japan  
[kobayashi@isl.sist.chukyo-u.ac.jp](mailto:kobayashi@isl.sist.chukyo-u.ac.jp)

Shuichi Akizuki  
Chukyo University  
101-2 Yagoto-honmachi  
466-8666, Nagoya, Japan  
[s-akizuki@sist.chukyo-u.ac.jp](mailto:s-akizuki@sist.chukyo-u.ac.jp)

Manabu Hashimoto  
Chukyo University  
101-2 Yagoto-honmachi  
466-8666, Nagoya, Japan  
[mana@isl.sist.chukyo-u.ac.jp](mailto:mana@isl.sist.chukyo-u.ac.jp)

## ABSTRACT

This paper proposes a natural data augmentation method and an anomaly removal artificial neural network for accurate anomaly detection. Anomaly detection is important because the provision of high-quality products is vital in the manufacturing industry. However, it is difficult to obtain a sufficient number of anomaly samples for the detection, which represents a significant challenge when it comes to achieving accurate anomaly detection by machine learning. General data augmentation methods generate new anomaly images by combining normal images and anomaly images. As an alternative, this paper describes a method that generates new anomaly images by using the Eigenspace. More natural anomaly images are generated than with general data augmentation methods. This paper also proposes an anomaly removal neural network that utilizes this natural data augmentation. The results of an anomaly detection experiment showed that the AUC of 94.7% was achieved for the capsule dataset when using anomaly images generated by the proposed data augmentation for training the anomaly removal neural network. This is 1.3% higher than the state-of-the-art data augmentation method that has been utilized for training the neural network. In the case of the pill dataset, AUC of 99.4% was achieved by proposed method. This is 3.0% higher than the state-of-the-art data augmentation method that has been utilized for training the neural network. The results of a series of experiments demonstrated that anomaly images generated by the proposed data augmentation are effective for training the neural network.

## Keywords

Anomaly detection, Machine learning, Image generation, Data augmentation, Principal component analysis, Eigenspace

## 1. INTRODUCTION

Recently, machine learning has shown promise for accurate anomaly detection. However, there is a shortage of anomaly images for learning due to the difficulty to obtaining such images in the manufacturing industry. This is a critical issue when it comes to achieving accurate anomaly detection.

Permission to make digital or hard copies of all or part of this work for personal or classroom use is granted without fee provided that copies are not made or distributed for profit or commercial advantage and that copies bear this notice and the full citation on the first page. To copy otherwise, or republish, to post on servers or to redistribute to lists, requires prior specific permission and/or a fee.

Conventionally, three approaches to address this issue have been taken. In the first approach, methods use reconstruction models based on Generative adversarial networks (GANs) [Sch17] [Zen18] [Akc19]. These methods aim to successfully reconstruct normal images, while unsuccessfully reconstructing anomalies. However, they may be able to successfully reconstruct an anomaly image because the models learn to reconstruct the input image.

In the second approach, methods utilize pre-trained Convolutional neural networks (CNNs) as feature extractors [Coh20] [Rip21] [Def21] [Rot22]. These methods aim to model the normal features for detecting anomaly features. However, since they do

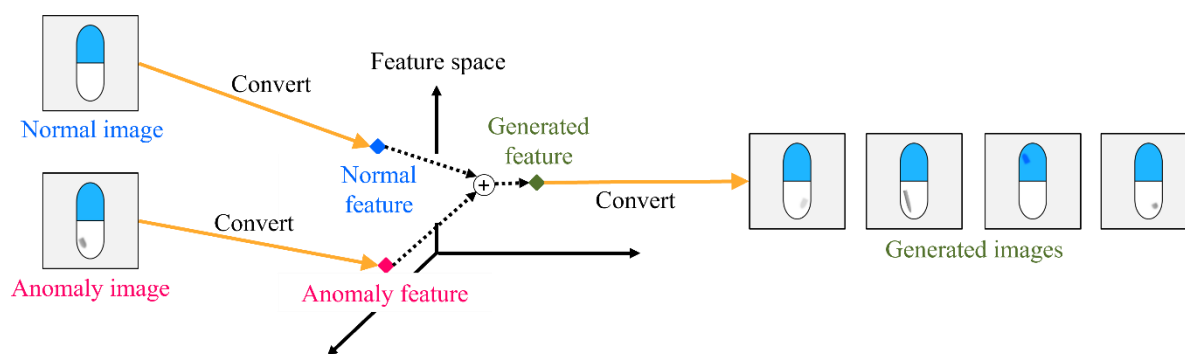


**Figure 1. Basic concept of proposed method.**

not learn anomaly images, they may miss very small anomalies.

In the third approach, methods generate artificial anomaly images by data augmentation. For example, CutPaste [Li21] trains the one-class discrimination of CNNs by using normal images and generated anomaly images. StainNoise [Col21], DRAEM [Zav21], and NSA [Sch22] train image reconstruction artificial neural networks using normal images and generated anomaly images and then determine anomalies from the input and output of the neural network. These methods can generate a lot of anomaly images by combining artificial anomalies and normal images. However, when the artificial anomalies are unnatural, artifacts may occur in the generated anomaly images, which affect the learning of the neural networks. In other words, if low-quality anomaly images are generated by the previous data augmentations, the accuracy of the subsequent anomaly detection may decrease.

Thus, Conventional data augmentation methods in the image space generate unnatural anomaly images. This is problematic for the quality of the training data. In this study, we propose a data augmentation method in the feature space instead of the conventional approach in the image space. Then, we propose a neural network for anomaly removal based on the data augmentation.

## 2. PREVIOUS DATA AUGMENTATION AND BASIC CONCEPT OF PROPOSED IDEA

In this section, we first describe the general approach to data augmentation and its issues. We then present our basic idea to address the problems of the previous methods.

### 2-1. Previous data augmentation methods and related problems

When applying machine learning to anomaly detection, it is necessary for the discriminator to learn various anomalies. However, there is a shortage of anomaly images for machine learning due to the

difficulty of obtaining a sufficient number of such images in the manufacturing industry.

In the field of anomaly detection, there are methods that generate anomaly images by combining artificial anomalies with normal images [Li21] [Col21] [Zav21] [Sch22]. These methods have the advantage of being able to generate the many anomaly images required for the training of discriminators. However, when the artificial anomalies are unnatural, artifacts may occur in the generated anomaly images, which in turn affects the learning of the discriminators. In other words, the problem here is that discriminators cannot acquire a generalizable performance with unnatural data augmentation. Our aim in this study is, therefore, to improve the quality of anomaly images generated by data augmentation.

### 2-2. Basic concept

Real images contain various information, such as the position of the object and the size of the anomalies. If we can extract and fuse these pieces of information from real images, we should be able to generate highly realistic anomaly images.

The basic concept is shown in Fig. 1. First, the images are converted into feature values, and next the normal feature values and anomaly feature values are fused in the feature space. Finally, high-reality anomaly images are generated by converting these feature values into images. Additionally, various anomaly images can be generated by applying transform processing to the anomaly feature values in the feature space.

## 3. PROPOSED METHOD

In this section, first, we explain our method of converting images into feature values using principal component analysis. Next, we present our method for combining normal feature values and anomaly feature values in the Eigenspace, along with our method for diversifying the anomaly information in the generated images. Finally, we show our method for training an anomaly removal neural network using normal images and generated anomaly images.

### 3-1. Feature transformation based on principal component analysis

In our approach, images are transformed into feature values by means of principal component analysis. There are two advantages to using principal component analysis for feature transformation: first, the feature values in the Eigenspace obtained in this way can be converted into images, and second, the feature values in the Eigenspace can be interpreted on the basis of the eigenvalues. Image generation methods utilizing the feature space include those using Variational Auto-Encoder (VAE) [Gar19] and GANs [Ant17] [Bow18]. However, since these methods use deep learning, it is difficult to interpret the features in the feature space.

Here, we transform images into features as follows. Principal component analysis is applied to  $N$  training images comprising many normal images and a small number of anomaly images. When the dimensionality of the image vectors is  $D$  dimensions ( $N < D$ ), the  $N$  image vectors  $\mathbf{x}_n$  ( $n = 1, 2, \dots, N$ ) are defined by

$$\mathbf{x}_n = (x_{n1}, x_{n2}, \dots, x_{nD})^T. \quad (1)$$

Next, the data is centered by taking the difference between the  $N$  image vectors  $\mathbf{x}_n$  and the mean vector  $\bar{\mathbf{x}}$ . The data matrix of the centered data  $\bar{\mathbf{x}}_n$  ( $n = 1, 2, \dots, N$ ) is defined by

$$\bar{\mathbf{X}} = (\bar{\mathbf{x}}_1, \dots, \bar{\mathbf{x}}_n)^T = (\mathbf{x}_1 - \bar{\mathbf{x}}, \dots, \mathbf{x}_n - \bar{\mathbf{x}})^T. \quad (2)$$

Using this data matrix  $\bar{\mathbf{X}}$ , the covariance matrix  $\mathbf{S}$  can be obtained by

$$\mathbf{S} = \frac{1}{N} \bar{\mathbf{X}}^T \bar{\mathbf{X}}. \quad (3)$$

In the principal component analysis, the eigenvalue problem for this covariance matrix  $\mathbf{S}$  is solved. As a result, the eigenvalues  $\lambda_j$  and the corresponding  $D$  dimensional eigenvectors  $\mathbf{a}_j$  are derived. When the dimensionality  $D$  is larger than the number of training images  $N$ , the number of non-zero eigenvalues and their corresponding eigenvectors obtained are  $N - 1$ .

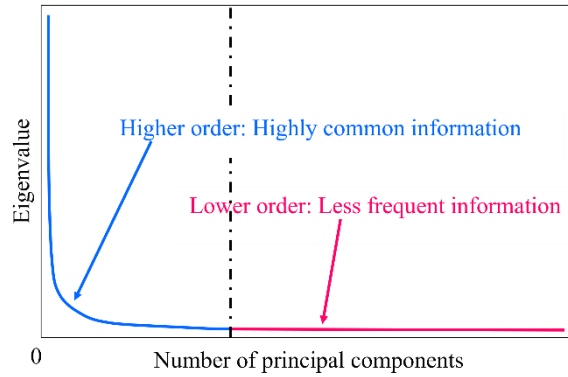


**Figure 2. Relationship between eigenvalues and principal component numbers.**

By selecting the eigenvectors  $\mathbf{a}_j$  corresponding to the eigenvalues  $\lambda_j$  in descending order, the Eigenspace  $\mathbf{A}$  is obtained. By projecting the centered image vectors  $\bar{\mathbf{x}}_n$  onto Eigenspace  $\mathbf{A}$ , the image is transformed into the feature vectors  $\mathbf{s}_n$ , which is defined by

$$\mathbf{s}_n = \mathbf{A}^T \bar{\mathbf{x}}_n = (s_{n1}, s_{n2}, \dots, s_{nN-1})^T. \quad (4)$$

### 3-2. Fusion of anomaly features in Eigenspace

Next, using pairs of centered normal image vectors  $\bar{\mathbf{x}}_{nor}$  and anomaly image vectors  $\bar{\mathbf{x}}_{ano}$ , new anomaly images  $\tilde{\mathbf{x}}_{ano}$  are generated.

First, using Eq. (4) from Subsection 3-1, we project the normal image vectors  $\bar{\mathbf{x}}_{nor}$  and the anomaly image vectors  $\bar{\mathbf{x}}_{ano}$  onto Eigenspace  $\mathbf{A}$ . As a result, the feature vectors  $\mathbf{s}_{nor}$  and  $\mathbf{s}_{ano}$  are obtained.

The relationship between the eigenvalues  $\lambda_j$  and the principal component numbers is shown in Fig. 2. Here, we expect the top components with large eigenvalues to aggregate normal information correlated with all the data, while in contrast, the lower components with small eigenvalues are expected to aggregate anomaly information, especially for anomaly images.

Therefore, for the feature vectors  $\mathbf{s}_{nor}$  obtained from the normal images, the top components of the feature

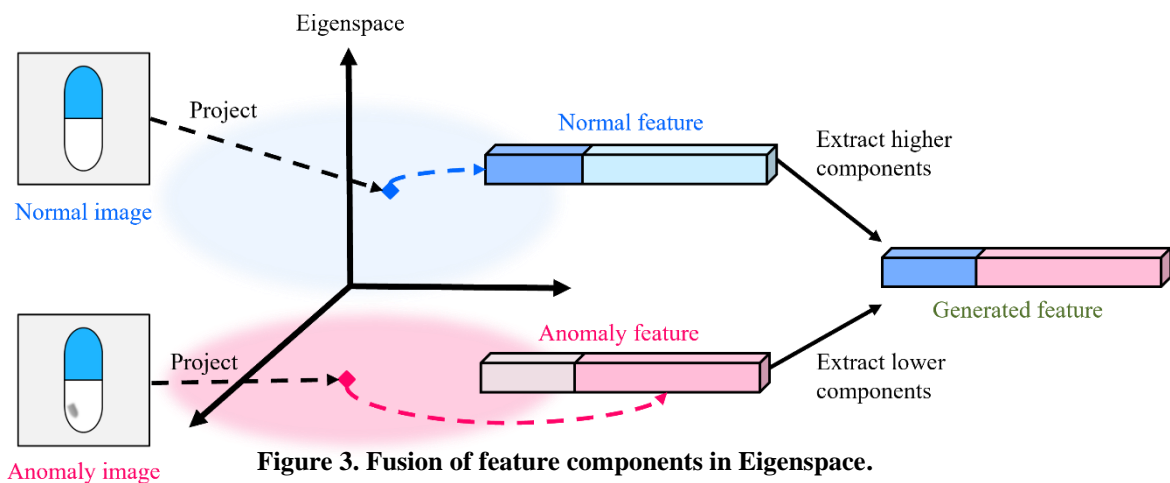


**Figure 3. Fusion of feature components in Eigenspace.**

vectors are extracted, and for the feature vectors  $s_{ano}$  obtained from the anomaly images, the lower components are extracted. In this case, the boundary between the top and bottom features is qualitatively determined from the cumulative contribution rate graph, defining the components up to the  $M$ -th component as the top and the rest as the bottom.

Finally, new features are generated by combining the extracted feature components in the Eigenspace. Fig. 3 shows the generation of new features by fusing the normal and anomaly feature vectors in the Eigenspace. These features are transformed into images by adding the mean vector  $\bar{x}$  to the linear combination of their components and each eigenvector, as

$$\tilde{x}_{ano} = \bar{x} + \sum_{i=1}^M s_{nor(i)} \mathbf{a}_i + \sum_{i=M+1}^{N-1} s_{ano(i)} \mathbf{a}_i \quad (5)$$

By this operation, a new anomaly image  $\tilde{x}_{ano}$  is generated by fusing the defect features of defective image  $x_{ano}$  into the normal image  $x_{nor}$ .

### 3-3. Diversification processing of anomaly information

Using Eq. (5) from Subsection 3-2, new anomaly images are generated by fusing anomaly information from anomaly images into normal images. However, the position and size of anomalies in the generated images depend on the anomaly images used for the image generation. Therefore, variation in the generated images is limited to the number of combinations of normal and anomaly images. In this subsection, we modify Eq. (5) to variate the generated anomalies. There are two targets for diversifying anomalies: anomaly intensity and geometric information.

First, we diversify the anomaly intensity in the generated images by multiplying the weight coefficient  $w$ , as

$$\tilde{x}_{ano} = \bar{x} + \sum_{i=1}^M s_{nor(i)} \mathbf{a}_i + w \sum_{i=M+1}^{N-1} s_{ano(i)} \mathbf{a}_i \quad (6)$$

Next, we describe the diversification of geometric information about anomalies. In Eq. (5), the linear combination of anomaly features and lower eigenvectors represents anomaly information. Therefore, this anomaly information vector is transformed into the image-size matrix. Then, geometric transformations such as mirroring and reduction are applied to this matrix. Then, this matrix is transformed into a vector and added to the normal information vector. As a result, the geometric information of the anomaly in the generated image changes.

### 3-4. Anomaly removal neural network

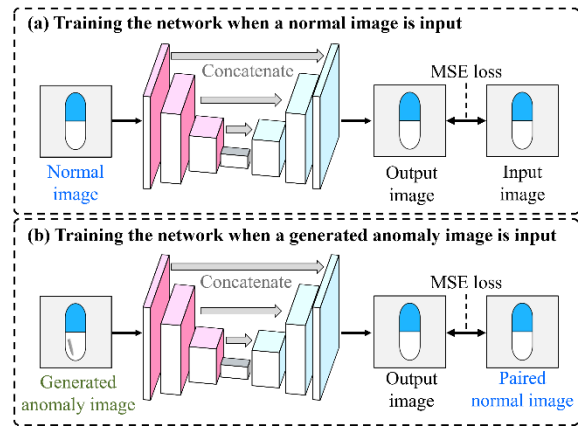


Figure 4. Training of anomaly removal neural network.

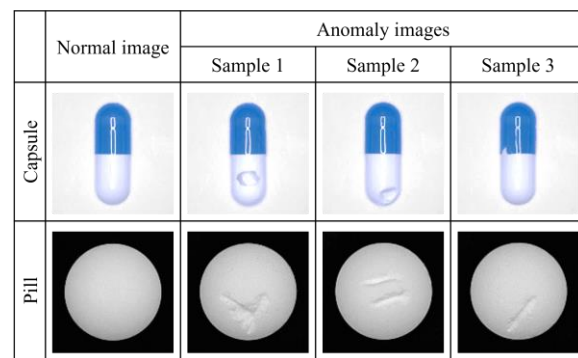


Figure 5. Example images of each dataset.

By using the data augmentation method described in Subsection 3-1 to Subsection 3-3, pairs of normal images and artificially generated anomaly images can be obtained. The artificially generated anomaly images in this pair are identical to the normal images except for the anomaly parts.

We then use this pair of images to train the anomaly removal neural network, as shown in Fig. 4. The neural network architecture utilizes U-Net [Ron15], which is a type of autoencoder. During the training, when a normal image is input, the Mean Squared Error (MSE) loss is calculated between the output  $y$  of the neural network and the normal image  $x_{nor}$  (Fig. 4(a)). When an artificial anomaly image generated using the proposed data augmentation is input, the MSE loss is calculated between the output  $y$  of the neural network and the normal image  $x_{nor}$  paired with this artificial anomaly image  $\tilde{x}_{ano}$  (Fig. 4(b)). The equation is shown below. As a result of this training, the anomaly removal neural network is obtained.

$$MSE = \frac{1}{nm} \sum_{j=0}^{n-1} \sum_{i=0}^{m-1} [y(j, i) - x_{nor}(j, i)]^2 \quad (7)$$

During the testing of the neural network, the anomaly score is defined as the sum of the absolute differences

between the input image  $x$  and the output image  $y$  of the neural network. The equation is shown below.

$$anomaly\ score = \sum_{j=0}^{n-1} \sum_{i=0}^{m-1} |y(j, i) - x(j, i)| \quad (8)$$

#### 4. IMAGE GENERATION EXPERIMENT

We performed an image generation experiment in which new anomaly images were generated by the proposed data augmentation method using many normal images and a few anomaly images. Our objectives are to determine whether (1) various anomaly images can be generated by the fusion of normal and anomaly features in the Eigenspace and (2) the anomaly areas in the generated images appear natural.

##### 4-1. Settings

We utilized the capsule dataset and the pill dataset comprising grayscale images sized  $128 \times 128$ . Example images are shown in Fig 5, depicted in color for display purpose. Note that, since principal

component analysis is used for image generation, the position of the objects has been aligned in advance.

In this experiment, we utilized 300 normal images and 15 anomaly images from the capsule dataset. We utilized 1200 normal images and 15 anomaly images from the pill dataset. New anomaly images were generated using the proposed data augmentation method. We checked a graph of the cumulative contribution rate obtained by principal component analysis. We determined to be the top component up to a cumulative contribution rate of 99.0% for the capsule dataset and determined to be the top component up to a cumulative contribution rate of 90.0% for the pill dataset. Regarding the diversification process applied to anomaly information, a combination of scalar transformation was utilized. The value of the scalar multiplication was determined randomly within the range of 0.8 to 1.0. The mirror transformation was randomly selected from among three types (vertical, horizontal, and combined vertical and horizontal). The reduction transformation ratio was set randomly within the range of 0.8 to 1.0.













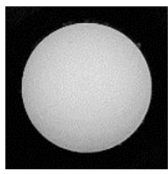
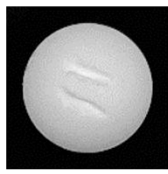
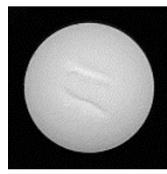
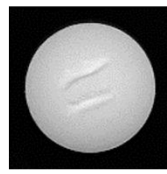
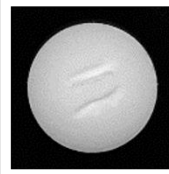
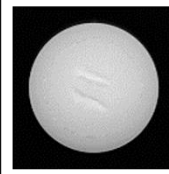
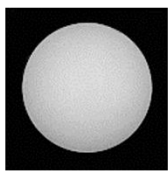
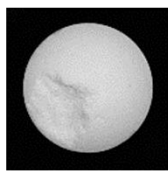
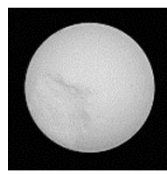
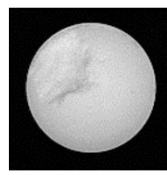
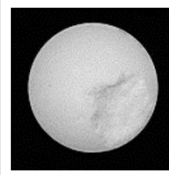
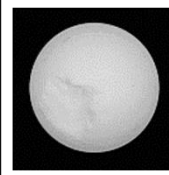
	Pair of real images		Examples of generated variations			
	Normal images	Anomaly images	Intensity	Geometry		
			Weight	Mirroring		Reduction
Capsule (1)						
Capsule (2)						
Pill (1)						
Pill (2)						

Figure 6. Results of image generation.



## 4-2. Results

Fig. 6 shows examples of pairs of normal images and anomaly images used for image generation, along with the generated images from those pairs. Note that, as in Fig.5, the images here are actually grayscale, but are depicted in color for display purpose. In terms of computation time (CPU: Intel Core i7-12700KF, Memory: 32 GB), Principal component analysis took 1566 sec, and generating 300 images took 442 sec for the capsule dataset.

The results of the capsule dataset in Fig. 6 show that new images have been generated by fusing the anomaly information from anomaly images onto normal images. Specifically, when the anomaly intensity is diversified, the anomaly intensity of the generated images changes compared to that of the anomaly images used for the data augmentation. Additionally, when the position of the anomaly is diversified by mirror transformation, the position of the anomaly in the anomaly images used for the data augmentation differs from in the generated images. At this time, only the position of the anomaly has changed, while the position of the capsule remains unchanged. When the size of the anomaly is diversified by reduction transformation, the anomalies in the generated images are smaller compared to those in the anomaly images used for the data augmentation. At this time, only the size of the anomaly has changed, while the size of the capsule itself remains unchanged. This is because the normal information and anomaly information have been appropriately extracted in the Eigenspace. Further, focusing on the anomaly area of the generated images, we can see that the boundary between the anomaly and the object is natural and that highly realistic anomaly images have been generated. Similar results were confirmed from the pill dataset.

These results demonstrate natural data augmentation has been achieved by the fusion of normal and anomaly information in the Eigenspace.

## 5. ANOMALY DETECTION EXPERIMENT

In the next experiment, we investigated whether the anomaly images generated by the proposed data augmentation are effective as training data for the anomaly removal neural network.

### 5-1. Settings

We utilized the same capsule and pill datasets here as in Section 4 and compared the following four cases.

- 1) The discriminator has been trained using anomaly images generated by the proposed data augmentation.
- 2) The anomaly removal neural network has been trained with only normal images.

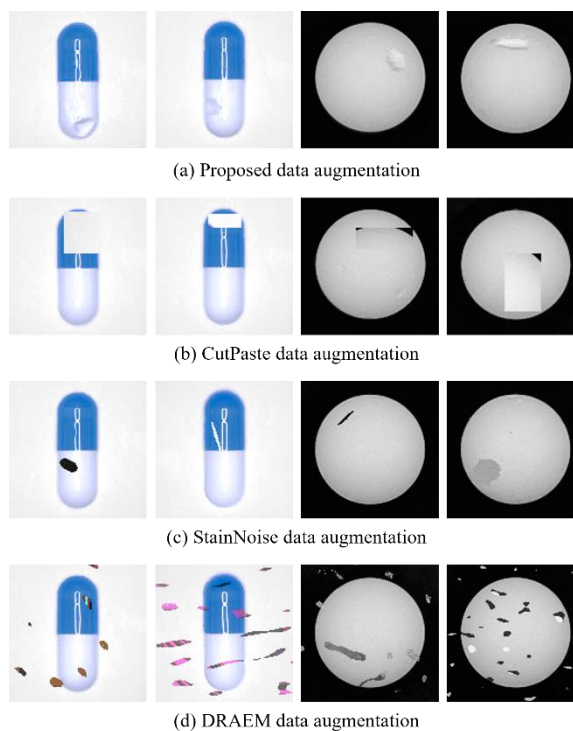


**Figure 7. Qualitative comparison of proposed and previous methods.**

	Capsule dataset			Pill dataset		
	Normal	Anomaly	Generated anomaly	Normal	Anomaly	Generated anomaly
Training ResNet using proposed method	300	0	300	1200	0	1200
Training U-Net using only normal image	300	0	0	1200	0	0
Training U-Net using previous method	300	0	300	1200	0	1200
Training U-Net using proposed method	300	0	300	1200	0	1200
Test	300	300	0	300	300	0

**Table 1. Number of images in anomaly detection experiment.**

- 3) The neural network has been trained using anomaly images generated by previous methods.
- 4) The neural network has been trained using anomaly images generated by the proposed data augmentation.

The previous methods we compared are CutPaste [Li21], StainNoise [Col21], and DRAEM [Zav21].

DRAEM is a state-of-the-art anomaly detection method using data augmentation.

Fig. 7 shows a comparison of the images generated by each method. CutPaste generates anomaly images by cutting out any rectangular region of a normal image and pasting it onto another area. StainNoise generates elliptical anomalies and synthesizes them into normal images to generate anomaly images. DRAEM generates anomalies from texture images of other

domains and synthesizes them into normal images to generate anomaly images. In this experiment, the previous methods used only the data augmentation part and used the same model as the proposed method for the training.

Table 1 breaks down the number of images used for training and testing the discriminator and the proposed method used 300 normal images and 300 artificial

anomaly images for training the neural network in the case of the capsule dataset. The 300 artificial anomaly images were generated using 15 real anomaly images and 300 normal images. In the case of the pill dataset, the proposed method used 1200 normal images and 1200 artificial anomaly images for training the neural network. The 1200 artificial anomaly images were generated using 15 real anomaly images and 1200

Data augmentation	Ours	Only normal	CutPaste	StainNoise	DRAEM	Ours
Model	ResNet	U-Net	U-Net	U-Net	U-Net	U-Net
AUC	85.2%	87.3%	90.3%	86.8%	93.4%	<b>94.7%</b>

**Table 2. Results of the anomaly detection experiment for the capsule dataset.**

Data augmentation	Ours	Only normal	CutPaste	StainNoise	DRAEM	Ours
Model	ResNet	U-Net	U-Net	U-Net	U-Net	U-Net
AUC	97.0%	63.7%	97.6%	99.4%	96.4%	<b>99.4%</b>

**Table 3. Results of the anomaly detection experiment for the pill dataset.**

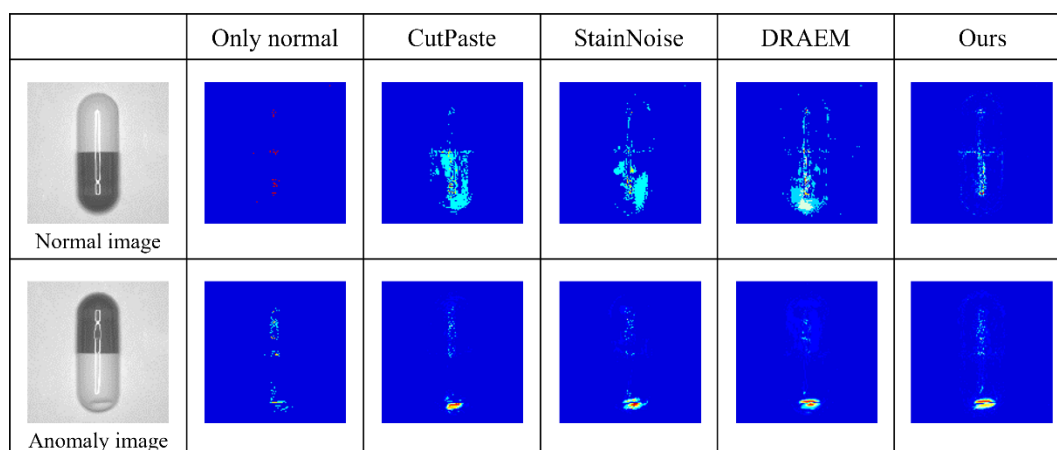


**Figure 8. Anomaly score maps output from the anomaly removal neural network for capsule dataset.**

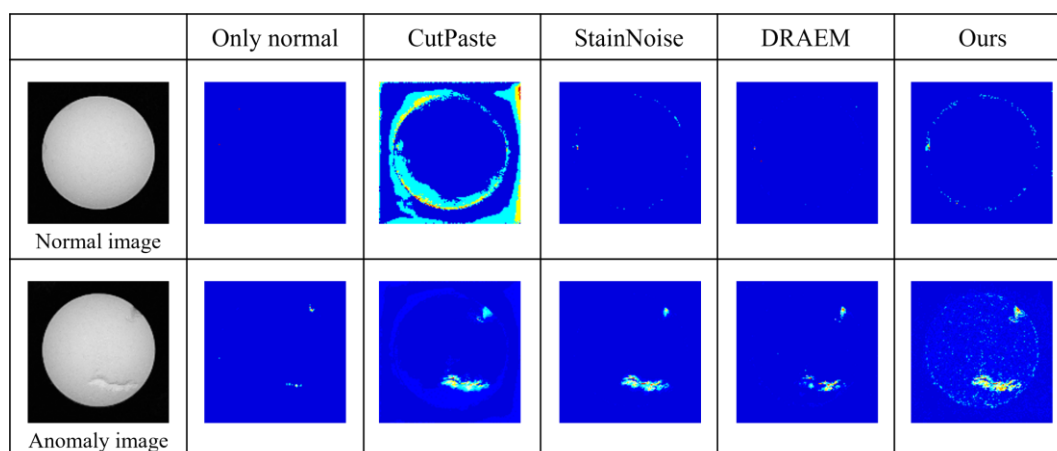


**Figure 9. Anomaly score maps output from the anomaly removal neural network for pill dataset.**

normal images. During testing, 300 normal images and 300 anomaly images were used.

Regarding the learning conditions, ResNet18 [He16] was used as the discriminator, and U-Net [Ron15] as the anomaly removal neural network. The batch size was set to 32 and the number of epochs was 300. The loss function for the discriminator was Binary Cross Entropy (BCE) loss. The loss function for the anomaly removal neural network was MSE loss. The optimization method was Adam [kin14] with the learning rate set to 0.0001. The anomaly detection performance was evaluated by the Area Under the Curve (AUC) during testing. AUC is the area under the ROC (Receiver Operating Characteristic) curve, which is created by calculating the true positive and false positive rates from the anomaly scores output from the neural network. Although the accuracy is also available as an evaluation indicator, AUC is more suitable from the viewpoint of threshold determination.

## 5-2. Results

The results of the anomaly detection experiments are listed in Table 2 and Table 3. Table 2 shows the experimental results for the capsule data set. Table 3 shows the experimental results for the pill dataset. From Table 2 (the capsule dataset), we can see the highest AUC of 94.7% was achieved when U-Net was trained using the proposed data augmentation. In contrast, the lowest AUC of 85.2% was achieved when ResNet18 was trained for class classification using the proposed data augmentation. From Table 3 (the pill dataset), we can see the highest AUC of 99.4% was achieved when U-Net was trained using the proposed data augmentation. In contrast, the lower AUC of 97.0% was achieved when ResNet18 was trained for class classification using the proposed data augmentation. The reason for the low result with ResNet is that, since its learning task is class discrimination, it was influenced by the number of real anomaly images used for the proposed data augmentation. Conversely, the anomaly removal neural network utilizing U-Net learns the task of removing anomalies from input images based on pairs of normal images and artificial anomaly images, so the influence of the number of real anomaly images used for the proposed data augmentation was minimal. These results indicate that when there are only a few real anomaly samples, training the proposed anomaly removal neural network can detect anomalies more accurately than class discrimination.

Furthermore, the proposed method had the highest AUC when compared with the case where the anomaly removal neural network was trained using artificially generated anomaly images by previous data augmentations. In the case of the capsule dataset, the proposed method is 1.3% higher than the result of DRAEM which is the state-of-the-art data

augmentation method. For the pill dataset, the proposed method is 3.0% higher than the result of DRAEM. Fig. 8 and Fig. 9 show the anomaly score map for input images when the anomaly removal neural network was trained using only normal images and when it was trained using each data augmentation method. First, when the anomaly removal neural network was trained only with normal images, the anomaly score map does not show any heat even when an anomaly image is input. This is because training the neural network only with normal images has given it the ability to output the same image as the input image. Next, when the anomaly removal neural network was trained using previous data augmentation methods, anomalies can be detected, but the anomaly score map also shows heat even when a normal image is input. In contrast, when the anomaly removal neural network was trained using the proposed data augmentation, anomalies can be detected and the anomaly score map does not show heat for the normal image. This is because the anomaly images generated by the proposed data augmentation are more natural than those generated by the previous data augmentation methods.

## CONCLUSION

In this study, we proposed a natural data augmentation method that generates natural anomaly images by fusing normal and anomaly features in the Eigenspace, along with an anomaly removal neural network based on this natural data augmentation. The results of an image generation experiment, demonstrate that natural anomaly images can be generated from pairs of many normal images and a few anomaly images. In addition, by applying transform processing to the anomaly features in the Eigenspace, various anomaly images can be generated. The results of an anomaly detection experiment show that the AUC of 94.7% was achieved for the capsule dataset when utilizing anomaly images generated by the proposed data augmentation for training the anomaly removal neural network, which is 1.3% higher than the state-of-the-art data augmentation method that was utilized for training the neural network. In the case of the pill dataset, the results of an anomaly detection experiment show that the AUC of 99.4% was achieved when utilizing anomaly images generated by the proposed data augmentation for training the anomaly removal neural network, which is 3.0% higher than the state-of-the-art data augmentation method that was utilized for training the neural network. These findings demonstrate that anomaly images generated by the proposed data augmentation are effective for training the anomaly removal neural network.



## 6. REFERENCES

- [Sch17] Schlegl, Thomas, et al. "Unsupervised anomaly detection with generative adversarial networks to guide marker discovery", International conference on information processing in medical imaging, pp.146-157, 2017.
- [Zen18] Zenati, Houssam, et al. "Efficient gan-based anomaly detection" arXiv preprint arXiv:1802.06222, 2018.
- [Akc19] Akcay, Samet, et al. "Ganomaly: Semi-supervised anomaly detection via adversarial training", Asian Conference on Computer Vision, pp. 622-637, 2019.
- [Coh20] Cohen, Niv, and Yedid Hoshen. "Sub-image anomaly detection with deep pyramid correspondences", arXiv preprint arXiv:2005.02357, 2020.
- [Rip21] Rippel, Oliver, et al. "Modeling the distribution of normal data in pre-trained deep features for anomaly detection", International Conference on Pattern Recognition, pp. 6726-6733, 2021.
- [Def21] Defard, Thomas, et al. "Padim: a patch distribution modeling framework for anomaly detection and localization" International Conference on Pattern Recognition, pp. 475-489, 2021.
- [Rot22] Roth, Karsten, et al. "Towards total recall in industrial anomaly detection" Proceedings of the IEEE/CVF Conference on Computer Vision and Pattern Recognition, pp. 14318-14328, 2022.
- [Li21] Li, Chun-Liang, et al. "Cutpaste: Self-supervised learning for anomaly detection and localization" Proceedings of the IEEE/CVF conference on computer vision and pattern recognition, pp. 9664-9674, 2021.
- [Col21] Collin, Anne-Sophie, et al. "Improved anomaly detection by training an autoencoder with skip connections on images corrupted with stain-shaped noise", International Conference on Pattern Recognition, pp. 7915-7922, 2021.
- [Zav21] Zavrtanik, Vitjan, et al. "Draem-a discriminatively trained reconstruction embedding for surface anomaly detection", Proceedings of the IEEE/CVF International Conference on Computer Vision, pp. 8330-8339, 2021.
- [Sch22] Schlüter, Hannah M., et al. "Natural synthetic anomalies for self-supervised anomaly detection and localization" European Conference on Computer Vision, pp. 474-489, 2022.
- [Gar19] Garay-Maestre, Unai, et al. "Data augmentation via variational auto-encoders", In Progress in Pattern Recognition, Image Analysis, Computer Vision, and Applications, pp. 29-37, 2019.
- [Ant17] Antoniou, Antreas, et al. "Data augmentation generative adversarial networks", arXiv preprint arXiv:1711.04340, 2017.
- [Bow18] Bowles, Christopher, et al. "Gan augmentation: Augmenting training data using generative adversarial networks" arXiv preprint arXiv:1810.10863, 2018.
- [Ron15] Ronneberger, Olaf, et al. "U-net: Convolutional networks for biomedical image segmentation", Medical image computing and computer-assisted intervention, pp. 234-241, 2015.
- [He16] He, Kaiming, et al. "Deep residual learning for image recognition", IEEE Conference on Computer Vision and Pattern Recognition, pp. 770-778, 2016.
- [Kin14] Kingma, Diederik P., et al. "Adam: A Method for Stochastic Optimization", arXiv preprint arXiv:1412.6980, 2014.

